

Superconducting and spin-density wave phases probed by scanning tunneling spectroscopy in the organic conductor $(\text{TMTSF})_2\text{ClO}_4$

Mohammadmehdi Torkzadeh,¹ Pascale Senzier,² Claude Bourbonnais*,³ Abdelouahab Sedeki,⁴ Cécile Mézière,⁵ Marie Hervé,¹ Francois Debontridder,¹ Pascal David,¹ Tristan Cren,¹ Claire Marrache-Kikuchi,⁶ Denis Jerome,² and Christophe Brun*¹

¹*Sorbonne Université, CNRS, Institut des Nanosciences de Paris, UMR7588, F-75252 Paris, France*

²*Laboratoire de Physique des Solides (UMR 8502) - Université Paris-Saclay, F-91405 Orsay, France*

³*Regroupement Québécois sur les Matériaux de Pointe and Institut Quantique,*

Département de physique, Université de Sherbrooke, Sherbrooke, Québec, Canada, J1K-2R1

⁴*Université Moulay Tahar de Saida, B.P. 138 cité ENNASR 20000, Saida, Algeria*

⁵*Univ Angers, CNRS, MOLTECH-Anjou, SFR MATRIX, F-49000 Angers, France*

⁶*Université Paris-Saclay, CNRS/IN2P3, IJCLab, 91405 Orsay, France*

(Dated: February 20, 2025)

By scanning tunneling microscopy (STM) we have probed the local quasi-particle density of states (DOS) of the Bechgaard salt organic superconductor $(\text{TMTSF})_2\text{ClO}_4$ in slowly cooled single crystals cleaved under ultrahigh vacuum conditions. In well STM imaged crystallographic surface planes, the local DOS has been probed for different surface areas at temperatures above and below the critical temperature of superconducting or insulating spin-density wave states. While a rather homogeneous superconducting state is expected in the bulk from previous studies, depending on the degree of disorder introduced by cleavage in the anion lattice, an inhomogeneous granular state is predominantly observed at the surface. A pronounced linear V-shape profile of the local DOS is observed from intermediate to the lowest energy scale in the less disordered superconducting surface areas. This supports the existence of an unconventional d-wave like order parameter with nodes at low energy, which is preceded by more energetic fluctuations attributed to quantum criticality of the material. At higher energy disorder combined to correlations deplete further the DOS. By contrast a non-linear U-shape characterizes the local low energy DOS profile for the more disordered and insulating surface areas of the spin-density wave state. The experimental results are compared quantitatively with those predicted by the renormalization group theory of the quasi-one dimensional electron gas model and its description of the superconducting and spin-density wave states that are interlinked by quantum criticality in the Bechgaard salts.

PACS numbers:

INTRODUCTION

Among the various families of unconventional superconductors discovered over the last four decades or so, organic materials occupy a noticeable place. This is well exemplified by the first organic superconductors to be synthesized, the Bechgaard salts $[(\text{TMTSF})_2X]$ series. These strongly anisotropic, quasi-one dimensional (quasi-1D), conductors are distinctive by the emergence of superconductivity on the edge of an insulating antiferromagnetic spin density-wave (SDW) state when pressure is tuned either hydrostatically or chemically from anion X substitution [1–3]. This sequence is now known as a classical example of pressure-tuned antiferromagnetic quantum critical point (QCP) made unstable by the development of a superconducting dome.

A major effort in the quest of understanding these materials has resided in explaining how both quantum criticality and superconductivity are reciprocally conditioned. To this end most sophisticated experiments have been conducted on $(\text{TMTSF})_2\text{ClO}_4$, the only member of the $(\text{TMTSF})_2X$ series displaying at ambient pressure a superconducting state below $T_c = 1.2\text{K}$, which is lo-

cated in the immediate vicinity of the QCP. Anomalous-featured order parameter for superconductivity is illustrated in various situations. These are for instance given by the detrimental effect of non magnetic impurities on T_c [4, 5]; the power law temperature dependence of the NMR relaxation rate [6, 7] and of specific heat below T_c [8]; the Fermi surface gap profiling by angle-resolved field dependent specific heat and its \sqrt{H} field profile in the vortex state [8]. Combined with the suppression of the NMR Knight shift in the superconducting state at low field [7], these findings support the existence of a singlet order parameter for superconductivity with a nodal structure on the Fermi surface, probably d -wave. Other experiments like former specific heat measurements, thermal conductivity and μ -sr, however, do not accord with this view and rather support the existence of a nodeless gap along the Fermi surface [9–11].

The hallmarks of quantum criticality fanning out through the metallic state are found in different conditions. This is the case of the linear temperature dependence of electrical resistivity [12, 13]. Also known as Planckian dissipation [14, 15], it is present over almost two decades in temperature around T_c in the Bechgaard salts. Another imprint comes from NMR spin-lattice re-

laxation rate. Different set of experiments reveal the existence of pronounced antiferromagnetic spin fluctuations, extending from the lowest temperature to far beyond T_c in the metallic state and whose amplitude is tuned by the pressure distance from the QCP [2, 7, 16–19].

None of these observations address directly the spectroscopic properties of quasi-particles in the quantum critical metallic domain and how these modify when entering in the superconducting phase. It is the main motivation of the present work to address these important issues from the angle of tunneling spectroscopy that can probe the quasi-particle density-of-states in the metallic, superconducting and insulating phases [20].

Several attempts to this end have been performed in the past using different tunneling setups. Early experiments used a n -doped GaSb Schottky barrier evaporated onto a $(\text{TMTSF})_2\text{PF}_6$ single crystal down to 50 mK under a pressure of 11 kbar [21]. It provided evidence of a well developed gap $2\Delta \approx 3.6$ meV at the Fermi level, interpreted as a superconducting gap, persisting above T_c like a pseudo gap structure. Subsequent $(\text{TMTSF})_2\text{ClO}_4$ studies at ambient pressure revealed similar results for superconductivity and evidenced also the role of the cooling speed on ClO_4 anion disorder leading to a shift on the pressure axis and to the onset of an insulating SDW state. An estimation of the SDW gap of $2\Delta_{\text{SDW}} \approx 6$ meV was given [22]. Further planar tunneling SIS' experiment using $(\text{TMTSF})_2\text{ClO}_4$ -amorphous Si-Pb junctions, revealed a much smaller superconducting energy gap in the ordered state of $2\Delta \approx 0.8$ meV and an SDW gap of $2\Delta_{\text{SDW}} \approx 3.0$ meV for the anion disordered state [23].

Given the diversity of these results it turned out to be important to have a reliable spectroscopic tunneling method to perform a direct determination of the quasi-particle density of states (DOS) in the superconducting, metallic and SDW phases. The method we have used is very low temperature scanning tunneling microscopy/spectroscopy (STM/STS) after having cleaved the $(\text{TMTSF})_2\text{ClO}_4$ sample under ultrahigh vacuum. This technique has been widely used on inorganic conventional and unconventional superconducting materials [24], including layered organic superconductors [25, 26]; it also has proven to achieve molecular resolution when applied to Q1D organic charge transfer compounds [27].

In this work, we could for the first time succeed to image the elementary **(a,b)** planes of $(\text{TMTSF})_2\text{ClO}_4$ resulting from the in-situ cleavage and perform STS on these planes. The dI/dV tunneling conductance measurements performed at $T = 300$ mK revealed various types of regions that are consistent with either superconducting or SDW phases depending on disorder conditions. Due to the cleavage process inducing disorder in the ClO_4 lattice sites, superconducting regions are rarely found in the surface plane. Instead, an inhomogeneous granular state is predominantly observed at the surface. In rare surface superconducting regions,

the quasi-particle excitation spectrum in the meV energy range reveals a strongly V-shaped DOS presenting a finite residual DOS at the Fermi level. The shape of the local excitation spectrum measured by STS is consistent with an order parameter having a nodal d-wave structure rather than nodeless s -wave. In contrast SDW puddles reveal U-shaped excitation spectra consistent with a nodeless energy gap having larger values than superconducting regions. In the energy range above the superconducting gap and above T_c , the V-shaped depletion of the quasi-particle DOS persists up to intermediate energy where disorder and correlations govern the depletion of the DOS. In the few meV range, we show that our results are rather congruent with the predictions of the renormalization group approach to the quasi-1D electron gas model for the SDW to d -wave SC sequence of ground states exhibited across a QCP [28].

EXPERIMENTAL SET-UP

The STM/STS experiments were carried out in an ultra-high vacuum set-up having a base pressure in the low 10^{-11} mbar range. $(\text{TMTSF})_2\text{ClO}_4$ single crystals of about several mm lengths were selected and glued on stainless steel sample holders using silver epoxy. Above the free sample surface, cleavers were glued using silver epoxy. The $(\text{TMTSF})_2\text{ClO}_4$ single crystals were cleaved at room temperature inside the STM chamber and introduced into the cold STM head at a temperature of about 100 K. The samples were further cooled down to helium temperature. Between 45 K and 4.2 K the samples were slowly cooled down to maintain a cooling speed of about 1.5 K per hour in order to ensure a very good structural ordering of the ClO_4 ions and favor the bulk development of the superconducting phase. The STM/STS experiments were carried out at a base temperature of 300 mK using a homemade apparatus based on a ^3He single-shot cryostat [29–31]. Mechanically cut PtIr tips were used. The differential tunneling conductance dI/dV spectra were obtained from the numerical derivative of single $I(V)$ curves. The individual spectra were further convolved with a Gaussian filter compatible with the thermal broadening at 300 mK.

RESULTS

Figure 1 shows the result of a nicely cleaved $(\text{TMTSF})_2\text{ClO}_4$ sample. Panel a) shows a 400×330 nm² STM topography measured at $T = 300$ mK emphasizing several **(a,b)** crystallographic planes separated by elementary steps oriented along the **c** direction. This is corroborated by the $Z(X)$ profile measured along the black line and presented in panel b). This profile shows flat sections of molecular **(a,b)** planes separated by an average

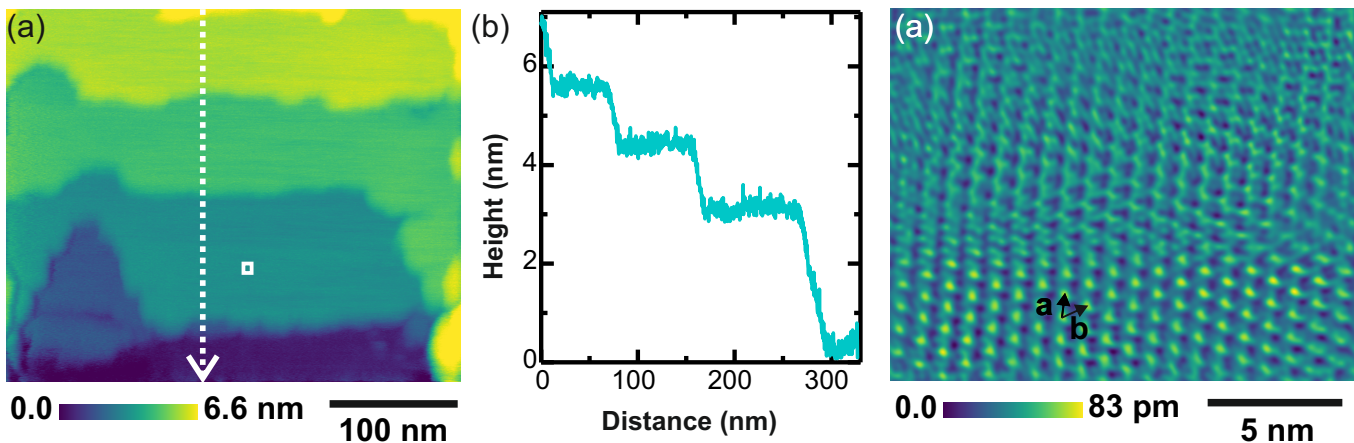


FIG. 1: (color online) Measurements performed at $T = 300$ mK. a) Raw color-coded constant current $Z(x, y)$ STM topography of a $(\text{TMTSF})_2\text{ClO}_4$ single-crystal cleaved under ultrahigh vacuum. The scanned area is $400 \times 330 \text{ nm}^2$ measured with $I = 50 \text{ pA}$ and $V_{\text{bias}} = -0.1 \text{ V}$. Several crystallographic (**a**,**b**) planes are seen. The color bar of $Z(x, y)$ expressed in nm is shown on the right. b) $Z(X)$ profile of the STM tip acquired along the line shown in black in image a). Both displacements Z and X are in nm. The height variations are consistent with the presence of elementary crystallographic steps along **c**. c) STM topography of a smaller area (of about $15 \times 15 \text{ nm}^2$), where molecular resolution could be obtained emphasizing the quasi-1D chains lying along **a**. The **b** direction is also indicated. The color bar of $Z(x, y)$ expressed in pm shows a corrugation less than 0.1 nm . This image was Fourier filtered to reduce the signal to noise ratio and highlight the molecular resolution.

c parameter of about $c \simeq 1.49 \text{ nm}$ as measured by STM locally in this particular area. It is consistent with the bulk reported value of 1.33 nm but presents an increase of about ten percent. This is a general observation that we made on other areas or samples. Additionally, on rare occasions, we have been able to obtain a clear molecular resolution on the (**a**,**b**) planes, as shown in panel c). Here, we clearly see the quasi-1D chains lying along **a**. Note that a tip change occurs in the bottom part of the image. Our results emphasize for the first time that the electronic properties of $(\text{TMTSF})_2\text{ClO}_4$ samples are accessible to STM/STS measurements if care is taken in the sample mounting and cleavage process.

Taking advantage of being able to scan crystallographic surface planes, we investigated the low-energy electronic properties of $(\text{TMTSF})_2\text{ClO}_4$ at various locations. The bulk critical temperature $T_c \simeq 1.2 \text{ K}$ was precisely determined from *ex-situ* electronic transport measurements on samples taken from the same batch, revealing a critical field $H_{C2-c^*} \approx 0.2 \text{ T}$ along \mathbf{c}^* , in good agreement with the literature (see section S1 supplementary material). Overall, our experimental results carried out on four different samples from the same batch all revealed inhomogeneous electronic properties at the surface, as measured by the STM/STS technique. This is in strong contrast to what can be expected from the T_c and bulk homogeneity of the electronic properties as probed using macroscopic techniques for a slow sample cooling speed [32?].

In the present work, we ascribe the electronic inhomogeneities observed at the surface to a structural disorder

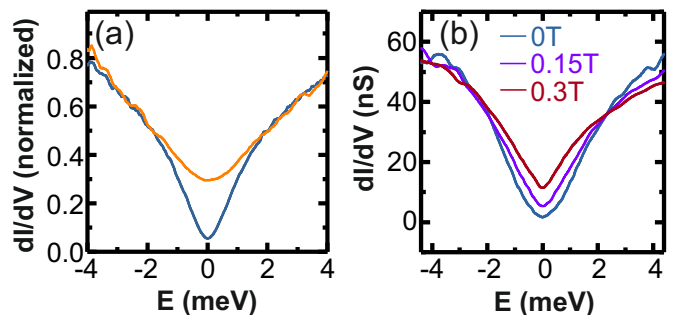


FIG. 2: (color online) Tunneling spectroscopic properties of $(\text{TMTSF})_2\text{ClO}_4$ cleaved under ultrahigh vacuum and acquired by scanning tunneling spectroscopy in the area shown on the lower terrace of the figure 1a). Differential tunneling conductance $dI/dV(E = eV_{\text{bias}})$ spectra measured in the energy range $[-4; +4] \text{ mV}$ with the following set-point for STS: $I = 300 \text{ pA}$ and $V_{\text{bias}} = -9 \text{ mV}$. Each presented spectrum is the average of a 60×60 STS grid measured at $T = 300 \text{ mK}$ (blue spectrum) or $T = 2.13 \text{ K}$ (yellow spectrum) over the same area of $8 \times 8 \text{ nm}^2$. b) Magnetic field dependence of the $dI/dV(E = eV_{\text{bias}})$ spectra at $T = 300 \text{ mK}$ with B applied along \mathbf{c}^* between 0 and 0.3 T (blue: 0 T , purple: 0.15 T , red: 0.3 T). The magnetic field dependence was probed in another sample area than the one probed in panel a).

induced in the anions sublattice. Indeed the ClO_4 ions are situated in-between (**a**,**b**) planes, so that the cleavage process should statistically remove part of these anions. Such an effect was already reported earlier by one of us in another well-known quasi-1D inorganic material, called the blue bronze, developing a charge-density wave

ground state where the ions are located in-between the molybdenum oxydes planes [33, 34]. In $(\text{TMTSF})_2\text{ClO}_4$ samples cleaved under ultrahigh vacuum we could identify at $T = 300$ mK different phases at the surface, including superconducting regions and SDW areas. In addition, other regions presenting correlated metallic states were also observed. We present below the characteristic tunneling spectra measured for each type of region.

Figure 2 shows differential tunneling conductance measurements performed both below T_c in the superconducting state and above T_c . The panel 2a) shows representative $dI/dV(E = eV_{\text{bias}})$ spectra measured at $T = 300$ mK (blue spectrum) and at $T = 2.13$ K (yellow spectrum), in zero-field cooled sample, in a 8×8 nm² region located in the lower terrace of the sample area seen in Fig.1a) indicated by a white square. The comparison between these two spectra enables to associate the internal dip structure of the 300 mK spectrum to the superconducting local density-of-states (LDOS). This is confirmed by the panel 2b) presenting the magnetic field dependence of the dI/dV spectra at $T = 300$ mK for a magnetic field applied along \mathbf{c}^* up to 0.3 T. A continuous increase of the conductance around E_F is observed with increasing magnetic field. A maximum of conductance is achieved around 0.25-0.3 T that we attribute to the surface critical field along \mathbf{c}^* H_{C2S} . This is in good quantitative agreement with bulk $H_{C2} \approx 0.2$ T measurements [8] as well as our own electrical resistivity measurements along \mathbf{c}^* (see section S1 in the supplementary material). We provide in the supplementary material other dI/dV spectra showing similar superconducting characteristics but emphasizing various gap filling, measured on other areas or samples (see section S4 in the supplementary material).

The figure 3 presents a typical tunneling spectrum, acquired in the same superconducting region as the low-energy spectra presented in panel 2a), but over a much larger energy range of about 50 times the superconducting energy gap. It is seen that the characteristic spectrum is strongly V-shaped up to more than 40 meV.

Figure 4 presents an interesting situation of local inhomogeneous electronic properties. It features a 40×13 nm² region where a spin-density wave puddle of size 15-20 nm (blue/darker area in panel b) is comprised between two superconducting areas (red-yellow-green/brighter area in panel b). The local tunneling spectra (blue and red/lighter colors in panel c) corresponding to the superconducting areas are similar to the one presented in figure 2a) but reach zero conductance very close to zero energy. In contrast, the middle area presents a strongly U-shaped spectrum (black curve) with a concavity that is opposite to the one of the superconducting spectra. Moreover, this U-shaped spectrum presents a larger energy gap and a lower conductance around the Fermi level reaching zero at E_F . In order to further support this result, we heuristically fitted all dI/dV spectra acquired over a 92×29 grid in this area, assuming a power law

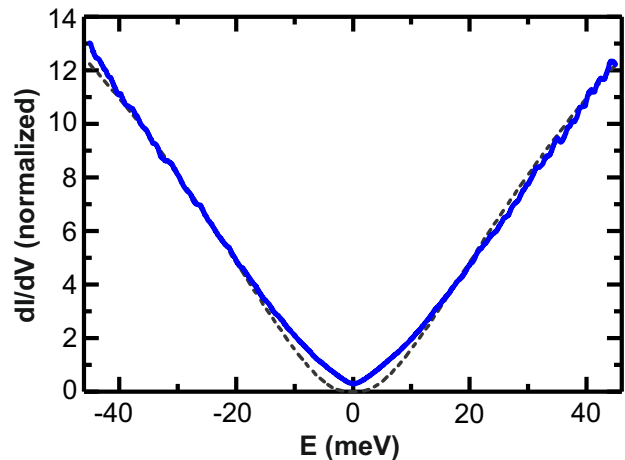


FIG. 3: (color online) Tunneling spectroscopic properties of $(\text{TMTSF})_2\text{ClO}_4$ acquired by scanning tunneling spectroscopy in the area shown on the lower terrace of the figure 1a), where the superconducting spectra shown in Fig. 2a) were also acquired. Differential tunneling conductance $dI/dV(E = eV_{\text{bias}})$ spectra measured in the energy range $[-40; +40]$ meV with the set-point: $I = 300$ pA and $V_{\text{bias}} = -40$ mV. The presented spectrum (continuous thicker curve) is the average of a 60×60 STS grid measured at $T = 2.13$ K over a 8×8 nm² area. The same normalization procedure as in Fig. 2a) is applied. Comparison with the Anderson-Hubbard model (dashed thinner curve), modelling the influence of disorder on the DOS at high energy, see text.

energy dependence in the form $dI/dV(E) \propto E^\eta$. The extracted exponent map $\eta(x, y)$ is presented in panel a). It anti-correlates with the conductance map of panel b): The larger the local exponent $\eta(x, y)$ (SDW puddle) the smaller the local conductance around -2 meV. Our result is in line with the reported SDW energy gap of about 3 meV [23] to 6 meV [22]. Further analysis of the experimental local exponent variations shown in panel 2a) enables to extract a superconducting and SDW coherence length of about 5 nm along the chain direction, implying a low mean-free path of about 1 nm. As we will see below, these low values with respect to the bulk clean limit ones, are consistent with the high broadening parameter required to fit the single-particle spectra. We have found numerous SDW puddles at the surface, additional examples being presented in the supplementary material (see section S5).

In addition to the superconducting and SDW puddles we have also found local regions where the tunneling spectra present only a correlated V-shaped background at large energy but without a clear signature of superconducting dip or SDW gap at low energy. Such regions could correspond to puddles of weakened or destroyed superconductivity having additional in-gap filled states, as for instance proposed in a variable-cooling transport study to describe a granular superconducting network [32]. Examples of this case are shown in supplementen-

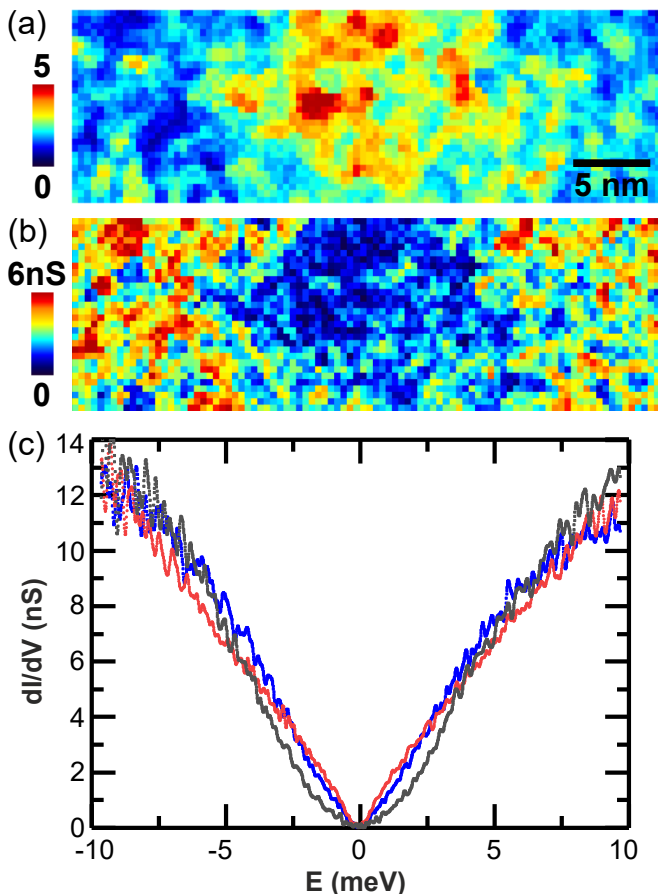


FIG. 4: (color online) Measurements done at $T = 300$ mK. a) Spatial map presenting the exponent η fitted from individual $dI/dV(E)$ spectra assuming the energy dependence $dI/dV(E) \propto E^\eta$ acquired on a 92×29 grid on a 40×13 nm² area. The scale bar is indicated. b) Differential tunneling conductance $dI/dV(E)$ map plotted at -2 meV, measured over the same 13×40 nm² area, extracted from a full $I(V)$ grid in the energy range [-10;+10] mV with the set-point for STS $I = 300$ pA and $V_{bias} = -9$ mV. Three different neighboring regions are seen: left superconducting (red-yellow-green/brighter), middle spin-density-wave (blue/darker region), right superconducting (red-yellow-green/brighter). c) Representative $dI/dV(E)$ spectra averaged locally in each left, middle, right area of the conductance map presented in panel b). Each spectrum is the average of about 50 single spectra.

tary section S6. Finally, we have also encountered several locally insulating planes at the surface, where it was not possible to perform STS of the low-energy spectrum. In such cases, the STM tip dug several nanometers or tens of nanometers into the interior of the material in order to find low-energy conducting planes satisfying a set-point such as $I = 200$ to 300 pA and $V_{bias} = -5$ to -9 mV. We interpret such situations as damaged/defected surface parts of the sample where some regions of the surface crystallographic planes are electrically badly con-

nected to bulk parts preventing the establishment of a tunneling current at low voltages. An example of such a situation is provided in the supplementary material (section S3), where the area could be imaged using a larger bias voltage before and after the tip dug into the surface while performing low-energy STS.

We summarize as follows the general observations that could be inferred from our numerous investigations :

- i) Superconducting regions are fewer at the surface plane than expected in the bulk.
- ii) Superconducting coherence peaks are strongly smeared out.
- iii) In the superconducting regions, the zero-bias conductance i.e. the LDOS at the Fermi energy, is most often finite and strongly fluctuates from one location to another.
- iv) In the SDW regions, the single-particle excitation spectra are U-shaped and reach zero at the Fermi energy.
- v) The normal state presents a strong V-shape background extending to energies at least two decades above the superconducting energy gap.

THEORY AND DISCUSSION

From electronic bandstructure calculations, a strongly V-shaped LDOS is not expected around E_F [35]. The existence of a quasi-1D bandstructure could lead to a k_{\parallel} tunneling dependence but not as strong as to induce such a fast increase of conductance as observed in our case over only 40 meV assuming a reasonable sample work function of at least one eV. A more convincing explanation is that we measure an intrinsic V-shaped LDOS due to the strongly correlated quasi-1D character of the LDOS combined to a rather large surface disorder associated to an inhomogeneous granular state. This emerges by first noting that the pronounced background depletion of LDOS seen up to at least 40 meV in Fig. 3 is not uncommon in disordered materials [36–39], including layered organic superconductors [25, 26]. These are characterized by sizable electron-electron interactions that can couple to disorder and then alter the density of states over relatively large energy scales. The perturbative approach of Altshuler and Aronov to this form of coupling is well known to produce such a suppression of the tunneling density of states [40]. Analogous features can also be found from a numerical treatment of the disordered Anderson-Hubbard model [41, 42]. These conditions are likely to be fulfilled for a compound as $(\text{TMTSF})_2\text{ClO}_4$ in which quantum criticality linking superconductivity to a correlated antiferromagnetic insulating state is occurring in the presence of non magnetic defects of the anion ordering. As shown below, the coupling of electron-electron interaction to randomness is responsible for the shaping of LDOS in energy down to 10 meV or so.

We follow the numerical approach of Ref. [41] to the Anderson-Hubbard model with the expression for the DOS in two spatial dimensions,

$$N_{\text{AH}}(E) = c \exp \left[-\alpha \ln^2 \left(\sqrt{2}|E|/E_F \right) \right], \quad (1)$$

where c and α are positive constants and E_F is the Fermi energy which is typically $E_F \simeq 0.26$ eV for a quasi-1D metal like $(\text{TMTSF})_2\text{ClO}_4$ [1]. Using a value of $\alpha \simeq 0.3$, the above expression fits fairly well the data of Fig. 3 over the whole range of intermediate energy. The value of α is comparable to the one found in layered organic superconductors showing a similar DOS depletion at intermediate energy [26]. However, the data do not evolve to the formation of a soft Hubbard gap as predicted to take place by the model around the Fermi level when the disorder-free electron system is a correlated insulator with a sharp gap. Deviations found below $E_0 \sim 10$ meV come from the onset of coherent quasi-particle states with a finite DOS on which our model developed below is based.

Below E_0 , the measured energy dependence of the STS spectra of Figures 2 and 4, associated with superconducting regions, is linear-like all the way down to the energy gap region. There, the LDOS is most often finite at zero E as in fig 2 (see also fig. 4 of the supplementary material) which is in agreement with macroscopic specific heat measurements [8, 43], but can also reach zero locally as in fig 4. This is not consistent with an s -wave nodeless order parameter but reminds what is observed in d -wave cuprates superconductors by STS [24]. Furthermore, non-magnetic disorder in the ClO_4 anions lattice can be expected to create local defects, as a result of the cleaving process. A more natural explanation compatible with point group symmetry would then be a d -wave symmetry where line nodes would give a linear energy dependent DOS in the superconducting energy gap, consistent with angular specific heat measurements [8, 24]. Moreover for a d -wave symmetry non-magnetic point defects behave as pair breakers, leading to additional gap filling, as predicted for a d -wave superconductor with impurity scattering in the unitary limit [44, 45] and often observed experimentally.

In the interpretation of the whole low energy part of the STS spectrum below E_0 , we shall adopt the view that SC and SDW states of the Bechgaard salts are the result of repulsive interactions alone, as approached by the theory of quasi-1D electron gas model. This model is based upon an electron spectrum with strongly anisotropic near- and next to near- neighbor transfer integrals. These lead to an open Fermi surface on which a set of electron-electron scattering amplitudes or coupling constants g_i can be defined. We shall make use of the extensive studies of renormalization group (RG) method for this model [19, 28, 46] (See also Supplementary material section S8). At the one-loop level for instance, these give a very reasonable description of the actual sequence of instabilities of the metallic state against SDW and

SC (d -wave) orders as the antineesting namely, the interchain next-to-nearest neighbor hopping parameter, t'_\perp , is tuned to simulate the influence of pressure. This occurs together with a dome of SDW quantum critical fluctuations that permeate deeply the metallic phase and whose amplitude scales with the one of T_c under pressure.

At the two-loop level of the RG, the one-electron spectral properties of the quantum critical domain of the model can be obtained. This the case of the energy profile of the DOS (normalized by the bare part N_0), $\bar{N}_n(E) = -\frac{2}{N_0\pi} \frac{1}{V} \sum_{\mathbf{k}} \text{Im} G(\mathbf{k}, E)$, which is linked to the coherent part of the one-particle retarded Green function G , as a function of wave vector \mathbf{k} and energy distance E from the Fermi level. Its renormalization is governed by the diagrammatic RG equation $\mathcal{O}(g_i^2)$ for the self-energy [28], as portrayed in Fig. 8 of Sec. S8 of Supplementary material. The local DOS probed by single particle tunneling, $\bar{N}_n(E) = \langle z(k_\perp, E) \rangle_{k_\perp}$, is expressed in terms of the energy dependent quasi-particle weight z averaged over the transverse wavevector k_\perp . In the metallic phase for $T > T_{c,\text{SDW}}$ calculations predict a drop of $\bar{N}_n(E)$ upon decreasing $|E|$ that is well described by a power law

$$\bar{N}_n(E) \propto (\text{Max}\{\pi k_B T, |E|\})^\eta, \quad E < 2t'_\perp \quad (2)$$

for low energy up to the scale of antineesting $2t'_\perp$ of the order of 5 meV for a quasi-1D compound like $(\text{TMTSF})_2\text{ClO}_4$ (see Sec. 8 of supplementary material). This scale marks the onset of an interplay between SDW and d -wave pairing fluctuations that initiates the low energy quantum critical domain. At higher energy for $E > 2t'_\perp$, the calculations show a transient weaker energy dependence of $\bar{N}_n(E)$ (See for instance Fig. 5). The latter evolves towards the higher energy scale of the nearest neighbor interchain hopping $t_\perp \sim 10t'_\perp \sim E_0$, located in turn at the onset of randomness scale for the DOS. In the low energy sector of interest, the exponent $\eta(t'_\perp)$ is non universal being t'_\perp or pressure dependent. Close to the QCP where SC emerges on the brink of SDW, $t'_\perp \simeq t'^*_\perp$ and $\eta(t'^*_\perp) \simeq 1$ with $\bar{N}_n(E)$ exhibiting a linear energy profile. On the SDW side of the phase diagram, at lower $t'_\perp < t'^*_\perp$, $\eta(t'_\perp) > 1$ increases above unity and $\bar{N}_n(E)$ shows a concave U-shape behavior in energy for temperature $T > T_{\text{SDW}}$ in the metallic state. By contrast, moving away from the QCP on the SC side, $\eta(t'_\perp)$ decays below unity, a drop that correlates with the one of T_c with t'_\perp . The influence of non magnetic impurity scattering on $\bar{N}_n(E)$ is here neglected since its impact on the strength of electron correlations of the quantum critical domain can be considered to be small [47].

At sufficiently low $|E|$, the metallic $\bar{N}_n(E)$ will be connected to the suppression of the DOS following the opening of a gap Δ_μ from either $\mu = \text{SC}$ or SDW long-range

order. The normalized DOS will take the form

$$\bar{N}(E) = \bar{N}_n(\Delta_\mu, |E|) \left\langle \text{Re} \left\{ \frac{|E + i\Gamma|}{\sqrt{(E + i\Gamma)^2 - \Delta_\mu^2(k_\perp)}} \right\} \right\rangle_{k_\perp}, \quad (3)$$

where $\bar{N}_n(\Delta_\mu, |E|) \propto (\text{Max}\{\Delta_\mu, |E|\})^\eta$. The k_\perp -average in brackets is a normalized BCS expression for the DOS of the quasi-1D electron gas in the presence of a gap Δ_μ and the broadening Γ due to impurity scattering assumed to be pair-breaking for both orderings [45, 48].

The above expression for the DOS enters in the differential tunneling conductance at temperature T :

$$\frac{dI}{dV}(E) = G_{nn} \int_{-\infty}^{+\infty} \bar{N}(\omega) \left[-\frac{\partial f(\omega + eV)}{\partial(eV)} \right] d\omega + G_0, \quad (4)$$

where $E = eV$, $f(\omega)$ is the Fermi distribution, G_{nn} and G_0 are adjustable constants for the normal conductance and the finite LDOS at the Fermi level.

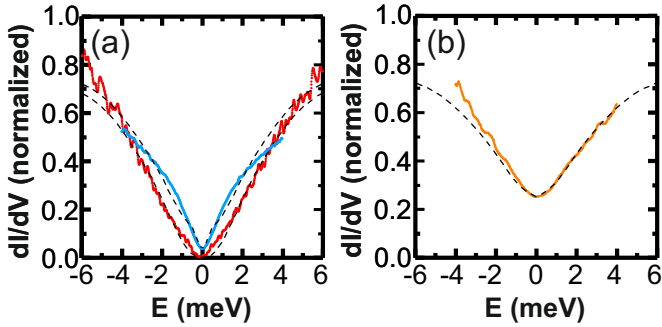


FIG. 5: Comparison of the renormalization group prediction (dashed dotted lines) and STM experiments for the density of states at (a): $T = 300$ mK in the SC state for the two regions shown in Figures 2 and 4, and (b): $T = 2$ K in the metallic state in the region shown in Figure 2-(a).

To fit the above expressions with the low energy STM data at $T = 300$ mK in the SC state, one substitutes the k_\perp -dependent, d -wave, superconducting gap $\Delta_{SC}(k_\perp) = \Delta_{SC} \cos k_\perp$ for an open quasi-1D Fermi surface, together with the RG results for $N_n(E)$ obtained from typical figures for the couplings g_i and band parameters for the Bechgaard salts [28] (See Sec. S8 of Supplementary material). These lead to a calculated critical temperature $T_c \simeq 1.1$ K at the value of antinesting pressure parameter $t'_\perp/k_B = 26$ K, namely close to the QCP, a value of the magnitude found experimentally in the bulk. The impact of impurity scattering on the ordering will be incorporated through the broadening factor Γ . The calculated energy profile of dI/dV is shown in Fig. 5-(a) with the STM data at $T = 300$ mK for the data of two different SC areas shown in Figures 2 and 4. The best fit is obtained for $\Gamma/\Delta_{SC} = 0.6$ and a ratio $\Delta_{SC}/k_B T_c = 8$ that exceeds by a factor about four the

BCS value for the SC state, a ratio known to be partly enhanced by impurity scattering [45]. The prediction gives a fair description of the differential conductance extending from the Fermi level up to $|E| \sim 5$ meV ($\gg \Delta_{SC}$). At $|E| < \Delta_{SC}$, this is consistent with a d -wave gap having nodes on the Fermi surface which leads to a linear dependence of the DOS on energy. No visible coherence peaks due to scattering rate Γ are found. This behavior then joins the E -linear DOS caused by quantum fluctuations spreading over a sizeable energy interval above the gap in accord with the RG solution close to the QCP.

In the normal phase above T_c , the $T = 2$ K data of the differential conductance of Fig. 2-(a) and reproduced in Fig. 5-(b) show a significant filling of the DOS expected by temperature effects close to the Fermi level. In that case Eq. (4) reduces to the normal state expression $(dI/dV)(E) \propto \bar{N}_n(E)$, where $\bar{N}_n(E)$ is given by the RG results (2) computed at $T = 2$ K with the same parameters that led to the T_c discussed above [28] (Sec. S8 of Supplementary material). $\bar{N}_n(E)$ is E -linear ($\eta \simeq 1$) outside the thermal broadening region at $|E| > \pi k_B T$ up to the beginning of the weaker energy transient dependence taking place from 5 meV or so. This behavior is congruent with the data of Fig. 5-(b) obtained up to 4 meV.

We now consider the results of the more disordered region where the system turns to be a SDW insulator at $T = 300$ mK, as displayed in Fig. 4 and reproduced in Fig. 6. In the phase diagram this would correspond to a negative shift along the pressure axis towards the SDW region. According to the figures, the data show a noticeable concavity or a U-shape form in energy for the DOS. This can be simulated theoretically by a downward shift of antinesting at $t'_\perp/k_B \simeq 25.4$ K in the phase diagram of the RG solution. An instability of the metallic state against SDW order then occurs at the critical temperature $T_{SDW} \simeq 5$ K, a magnitude typically found in quenched ClO_4 samples [49, 50]. In this SDW regime, the single particle gap $\Delta_{SDW}(k_\perp) \approx \Delta_{SDW}$ presents no nodes and can be taken as essentially momentum independent along the Fermi surface. From the fit in Fig. 6 obtained using $\Delta_{SDW}/k_B T_{SDW} = 3.6$ and $\Gamma/\Delta_{SDW} = 0.6$ in Eqs. (3-4), no coherence peaks for the DOS at $|E| \sim \Delta_{SDW}$ are found but a small kink is visible. This is followed by a U-shape E -profile below the gap scale, making scarcely visible the connection with the normal part (2) characterized by an exponent $\eta \simeq 1.3$ and a similar positive curvature in energy up to $2t'_\perp$.

It is worth noticing that the spatial map of the exponent η displayed in Fig. 4(a), show experimental values between 0.75 for superconducting regions and 5 for insulating ones. Such a range of η values is compatible with the ones found theoretically when the RG solution is carried out at slightly weaker or stronger t'_\perp/k_B around 26 K. When larger $\eta > 1$ values are encountered, stronger insulating SDW gaps take place (See Figs. 9-10 of sup-

plementary material) which is also observed experimentally (see Fig. 5 of supplementary material). However, it cannot be excluded that in these strongly insulating conditions the predictions of the disordered Anderson-Hubbard model can lead to results comparable to those of $\tilde{N}(E)$ in Eq. (3) for the DOS at low energy.

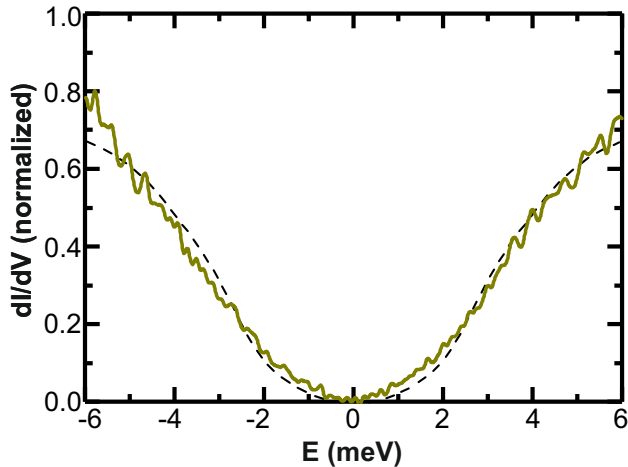


FIG. 6: Comparison of the renormalization group prediction (dashed line) and STM experiments of Fig. 4 for the density of states in the SDW state at $T = 300$ mK.

CONCLUSION

Since the discovery of the Bechgaard salts as the first series of organic superconductors, the nature of the superconducting order parameter in its prototype compound, $(\text{TMTSF})_2\text{ClO}_4$, has long framed a major part of the debate surrounding superconductivity in the series. Revealing the intricate link of superconductivity with bordering magnetic spin-density wave and quantum critical metallic phases has become another determinant issue regarding these materials.

The experimental and theoretical insights brought out by the present work have direct bearing upon these matters. Of particular note is the linear-like or convex low energy dependence of the local excitation spectra that has been probed by scanning tunneling spectroscopy. The linear profile appears to be akin to the Planckian linear temperature dependence of resistivity observed close to the QCP. The E-linear density of states is consistent with nodal d-wave rather than nodeless s-wave symmetry for the order parameter in the superconducting phase. By contrast, the concave energy dependence of the local excitation spectra, found in more disordered surface conditions, matches very well with the nodeless order parameter expected in an insulating spin-density wave phase.

Our experimental results find a quantitative support in the renormalization group approach to the quantum

critical precursors of both magnetic and superconducting orderings. This manifests itself through the prediction of a power law energy dependence E^η for the density-of-states at low-energy. The exponent η that characterizes metallic quantum fluctuations varies in relation with the nature of order in the low temperature phase. For superconductivity, $\eta \lesssim 1$ whereas $1 < \eta < 5$ for spin-density-wave, in definite connection with the surface mapping of tunneling conductance obtained in our experiments. This overall agreement between theory and experiments gives strong support for instabilities in the organic $(\text{TMTSF})_2\text{ClO}_4$ crystals as being primarily mediated by electron-electron repulsion combined to quantum criticality, resulting in nodal d-wave superconductivity and spin-density wave phases. Both phases are found to coexist in different regions of the surface, as a result of large anions disorder induced by the cleavage process.

ACKNOWLEDGEMENTS

We thank Claude Pasquier, Nicolas Dupuis and Shingo Yonezawa for fruitful discussion.

*christophe.brun@sorbonne-universite.fr,
Claude.Bourbonnais@USherbrooke.ca

-
- [1] D. Jérôme and C. Bourbonnais. Quasi one-dimensional organic conductors: from fröhlich conductivity and peierls insulating state to magnetically-mediated superconductivity, a retrospective. *Comptes Rendus. Physique*, 25:17, 2024.
 - [2] S.E. Brown. Organic superconductors: The bechgaard salts and relatives. *Physica C: Superconductivity and its Applications*, 514:279–289, 2015.
 - [3] Denis Jerome and Shingo Yonezawa. Novel superconducting phenomena in quasi-one-dimensional bechgaard salts. *Comptes Rendus Physique*, 17(3):357–375, 2016.
 - [4] N. Joo, P. Auban-Senzier, C. R. Pasquier, D. Jérôme, and K. Bechgaard. Impurity-controlled superconductivity/spin density wave interplay in the organic superconductor: $(\text{TMTSF})_2\text{ClO}_4$. *Europhys. Lett.*, 72:645, 2005.
 - [5] M. Y. Choi, P. M. Chaikin, S. Z. Huang, P. Haen, E. M. Engler, and R. L. Greene. Effect of radiation damage on the metal-insulator transition and low-temperature transport in the tetramethyltetraselenofulvalinium PF_6 salt $[(\text{TMTSF})_2\text{PF}_6]$. *Phys. Rev. B*, 25:6208–6217, 1982.
 - [6] Masashi Takigawa, Hiroshi Yasuoka, and Gunzi Saito. Proton spin relaxation in the superconducting state of $(\text{tmtsf})_2\text{clo}_4$. *Journal of the Physical Society of Japan*, 56(3):873–876, 1987.
 - [7] J. Shinagawa, Y. Kurosaki, F. Zhang, C. Parker, S. E. Brown, D. Jérôme, K. Bechgaard, and J. B. Christensen. Superconducting state of the organic conductor $(\text{TMTSF})_2\text{clo}_4$. *Phys. Rev. Lett.*, 98:147002, 2007.
 - [8] S. Yonezawa, Y. Maeno, K. Bechgaard, and D. Jerome. Nodal superconducting order parameter and thermody-

- namic phase diagram of $(\text{tmtsf})_2\text{clo}_4$. *Phys. Rev. B*, 85:140502(R), 2012.
- [9] P. Garoche, R. Brusetti, D. Jérôme, and K. Bechgaard. Specific heat measurements of organic superconductivity in $(\text{TMTSF})_2\text{ClO}_4$. *J. Physique Lettres*, 43:L-147, 1982.
- [10] S. Belin and K. Behnia. Thermal conductivity of superconducting $(\text{TMTSF})_2\text{clo}_4$: Evidence for a nodeless gap. *Phys. Rev. Lett.*, 79:2125, 1997.
- [11] F. L. Pratt, T. Lancaster, S. J. Blundell, and C. Baines. Low-field superconducting phase of $(\text{TMTSF})_2\text{clo}_4$. *Phys. Rev. Lett.*, 110:107005, 2013.
- [12] Nicolas Doiron-Leyraud, Pascale Auban-Senzier, Samuel René de Cotret, Claude Bourbonnais, Denis Jérôme, Klaus Bechgaard, and Louis Taillefer. Correlation between linear resistivity and T_c in the bechgaard salts and the pnictide superconductor $\text{Ba}(\text{Fe}_{1-x}\text{Co}_x)_2\text{as}_2$. *Phys. Rev. B*, 80:214531, 2009.
- [13] N. Doiron-Leyraud, S. René de Cotret, A. Sedeki, C. Bourbonnais, L. Taillefer, P. Auban-Senzier, D. Jérôme, and K. Bechgaard. Linear- t scattering and pairing from antiferromagnetic fluctuations in the $(\text{tmtsf})_{2x}$ organic superconductors. *Eur. Phys. J. B*, 78:23, 2010.
- [14] A. Legros, S. Benhabid, W. Tabis, F. Laliberté, M. Dion, M. Lizaïre, B. Vignolle, D. Vignolles, H. Raffy, Z. Z. Li, P. Auban-Senzier, N. Doiron-Leyraud, P. Fournier, D. Colson, L. Taillefer, and C. Proust. Quantum criticality. *Nature Physics*, 15:142, 2019.
- [15] J. A. N. Bruin, H. Sakai, R. S. Perry, and A. P. Mackenzie. Similarity of scattering rates in metals showing t -linear resistivity. *Science*, 339:804, 2013.
- [16] F. Creuzet, C. Bourbonnais, L. G. Caron, D. Jérôme, and A. Moradpour. 77se nmr spin-lattice relaxation rate properties in the $(\text{tmtsf})_{2x}$ series under pressure: cooperative phenomena and sdw transition. *Synth. Met.*, 19:277, 1987.
- [17] C. Bourbonnais, F. Creuzet, D. Jérôme, K. Bechgaard, and A. Moradpour. Cooperative phenomena in $(\text{tmtsf})_2\text{clo}_4$: an nmr evidence. *J. Phys. (Paris) Lett.*, 45:L755, 1984.
- [18] Y. Kimura, M. Misawa, and A. Kawamoto. Correlation between non-fermi-liquid behavior and antiferromagnetic fluctuations in $(\text{tmtsf})_2\text{pf}_6$ observed using ^{13}C -nmr spectroscopy. *Phys. Rev. B*, 84:045123, 2011.
- [19] C. Bourbonnais and A. Sedeki. Link between antiferromagnetism and superconductivity probed by nuclear spin relaxation in organic conductors. *Phys. Rev. B*, 80:085105, 2009.
- [20] E. L. Wolf. *Principle of electron tunneling spectroscopy, second edition*, volume 152. Oxford University Press, 2011.
- [21] C. More, G. Roger, J. P. Sorbier, D. Jérôme, M. Ribault, and K. Bechgaard. *J. Phys. (Paris) Lett.*, 42:L313, 1981.
- [22] A. Fournel, C. More, G. Roger, J. P. Sorbier, and C. Blanc. *J. Phys. Colloq.*, 44:C3 879, 1983.
- [23] H. Bando, K. Kjimura, H. Anzai, T. Ishiguro, and G. Saito. *Mol. Cryst. Liq. Cryst.*, 119:41, 1985.
- [24] Øystein Fischer, Martin Kugler, Ivan Maggio-Aprile, Christophe Berthod, and Christoph Renner. Scanning tunneling spectroscopy of high-temperature superconductors. *Rev. Mod. Phys.*, 353:79, 2007.
- [25] Daniel Guterding, Sandra Diehl, Michaela Altmeyer, Torsten Methfessel, Ulrich Tutsch, Harald Schubert, Michael Lang, Jens Müller, Michael Huth, Harald O. Jeschke, Roser Valentí, Martin Jourdan, and Hans-Joachim Elmers. Evidence for eight-node mixed-symmetry superconductivity in a correlated organic metal. *Phys. Rev. Lett.*, 116:237001, 2016.
- [26] Sandra Diehl, Torsten Methfessel, Ulrich Tutsch, Jens Müller, Michael Lang, Michael Huth, Martin Jourdan, and Hans-Joachim Elmers. Disorder-induced gap in the normal density of states of the organic superconductor $(\text{bedt-ttf})_2\text{cu}[\text{n}(\text{cn})_2]\text{br}$. *Journal of Physics: Condensed Matter*, 27(26):265601, 2015.
- [27] Z.Z. Wang, J.C. Girard, C. Pasquier, D. Jerome, and K. Bechgaard. Scanning tunneling microscopy in ttf-tcnq : Phase and amplitude modulated charge density waves. *Phys. Rev. B*, 67:R-121401, 2003.
- [28] A. Sedeki, D. Bergeron, and C. Bourbonnais. Extended quantum criticality of low-dimensional superconductors near a spin-density-wave instability. *Phys. Rev. B*, 85:165129, 2012.
- [29] L. Serrier-Garcia, J. C. Cuevas, T. Cren, C. Brun, V. Cherkez, F. Debontridder, D. Fokin, F. S. Bergeret, and D. Roditchev. Scanning tunneling spectroscopy study of the proximity effect in a disordered two-dimensional metal. *Phys. Rev. Lett.*, 110:157003, 2013.
- [30] C. Brun, T. Cren, V. Cherkez, F. Debontridder, S. Pons, D. Fokin, M.C. Tringides, S. Bozhko, L.B. Ioffe, B.L. Altshuler, and D. Roditchev. Remarkable effects of disorder on superconductivity of single atomic layers of lead on silicon. *Nature Phys.*, 10:544, 2014.
- [31] Christophe Brun, Tristan Cren, and Dimitri Roditchev. Review of 2d superconductivity: the ultimate case of epitaxial monolayers. *Superconductor Science and Technology*, 30(1):013003, 2016.
- [32] S. Yonezawa, C.A. Marrache-Kikuchi, K. Bechgaard, and D. Jerome. *Phys. Rev. B*, 97:014521, 2018.
- [33] C. Brun, J. C. Girard, Z. Z. Wang, J. Marcus, J. Dumas, and C. Schlenker. Charge-density waves in rubidium blue bronze $\text{rb}_{0.3}\text{Moo}_3$ observed by scanning tunneling microscopy. *Phys. Rev. B*, 72:235119, 2005.
- [34] E. Machado-Charry, P. Ordejon, E. Canadell, C. Brun, and Z.Z. Wang. *Phys. Rev. B*, 74(6):155123, 2006.
- [35] J.-P. Pouget P. Alemany and E. Canadell. *Phys. Rev. B*, 89:155124, 2014.
- [36] W. L. McMillan and Jack Mochel. Electron tunneling experiments on amorphous $\text{ge}_{1-x}\text{au}_x$. *Phys. Rev. Lett.*, 46:556-557, 1981.
- [37] G. Hertel, D. J. Bishop, E. G. Spencer, J. M. Rowell, and R. C. Dynes. Tunneling and transport measurements at the metal-insulator transition of amorphous nb: Si. *Phys. Rev. Lett.*, 50:743-746, 1983.
- [38] C. Carbillet, V. Cherkez, M. A. Skvortsov, M. V. Feigel'man, F. Debontridder, L. B. Ioffe, V. S. Stolyarov, K. Ilin, M. Siegel, D. Roditchev, T. Cren, and C. Brun. Spectroscopic evidence for strong correlations between local superconducting gap and local altshuler-aronov density of states suppression in ultrathin nbn films. *Phys. Rev. B*, 102:024504, 2020.
- [39] A. Richardella, P. Roushan, S. Mack, B. Zhou, D.A. Huse, D.D. Awschalom, and A. Yazdani. Visualizing critical correlations near the metal-insulator transition in $\text{ga}(1-x)\text{mn}(x)\text{as}$. *Science*, 327:665, 2010.
- [40] B.L. Altshuler, A.G. Aronov, and P.A. Lee. *Phys. Rev. Lett.*, 44(4):1288, 1980.
- [41] Hiroshi Shinaoka and Masatoshi Imada. Single-particle

- excitations under coexisting electron correlation and disorder: A numerical study of the anderson-hubbard model. *Journal of the Physical Society of Japan*, 78(9):094708, 2009.
- [42] Hiroshi Shinaoka and Masatoshi Imada. Soft hubbard gaps in disordered itinerant models with short-range interaction. *Phys. Rev. Lett.*, 102:016404, 2009.
- [43] S. Yano et al. to be published.
- [44] E. Puchkaryov and K Maki. Impurity scattering in d-wave superconductivity. unitary limit vesus born limit. *Eur. Phys. J. B*, 4:191–194, 1998.
- [45] Y. Suzumura and H. J. Schulz. Thermodynamic properties of impure anisotropic quasi-one-dimensional superconductors. *Phys. Rev. B*, 39:11398–11405, 1989.
- [46] J. C. Nickel, R. Duprat, C. Bourbonnais, and N. Dupuis. 73:165126, 2006.
- [47] A. Sedeki, P. Auban-Senzier, S. Yonezawa, C. Bourbonnais, and D. Jerome. Influence of carrier lifetime on quantum criticality and superconducting T_c of $(\text{TMTSF})_2\text{ClO}_4$. *Phys. Rev. B*, 98:115111, 2018.
- [48] R. C. Dynes, V. Narayanamurti, and J. P. Garno. Direct measurement of quasiparticle-lifetime broadening in a strong-coupled superconductor. *Phys. Rev. Lett.*, 41:1509–1512, 1978.
- [49] S. Tomic, D. Jérôme, P. Monod, and K. Bechgaard. Epr and electrical conductivity of the organic superconductor di-tetramethyltetraselenafulvalenium-perchlorate, $(\text{TMTSF})_2\text{ClO}_4$ and a metastable magnetic state obtained by fast cooling. *J. Physique Lett.*, 43:L-839, 1982.
- [50] H. Schwenk, K. Andres, and F. Wudl. Resistivity of the organic superconductor ditetramethyltetraselenafulvalenium perchlorate, $(\text{TMTSF})_2\text{clo}_4$, in its relaxed, quenched, and intermediate state. *Phys. Rev. B*, 29:500–502, 1984.